

Coexistence of spin glass type freezing and cooperative paramagnetic state in $\text{Sr}_3\text{MnTiO}_7$ S. Chowki,¹ S. Rayaprol,² A. Mukhopadhyay,¹ and N. Mohapatra^{1,*}¹*Indian Institute of Technology Bhubaneswar, Bhubaneswar, Odisha-751013, India*²*UGC-DAE Consortium for Scientific Research, Mumbai Centre, R-5 Shed, BARC Campus, Mumbai-400085, India*

(Received 10 July 2015; revised manuscript received 5 November 2015; published 10 December 2015)

We report on the unusual magnetic properties in a double layer Ruddlesden-Popper phase tetragonal $\text{Sr}_3\text{MnTiO}_7$ by the measurements of dc magnetization, heat capacity, and neutron diffraction data. Despite of a high Curie-Weiss temperature of 427 K, no long-range magnetic order was observed down to 3.5 K, below which the magnetic susceptibility $\chi(T)$ and thermodynamic results suggest the presence of a glassy phase in magnetism. By the analysis of the nonlinear component of dc susceptibility and the corresponding scaling behavior, it is shown that the nature of the magnetic state below 3.5 K is not a true conventional spin glass type. Moreover, the low temperature magnetic susceptibility and specific heat behavior were found to be strikingly similar to that of lightly doped spin liquid systems. On the basis of the above results, we predict the coexistence of correlated (spin liquid) and uncorrelated spin (spin glass) states in $\text{Sr}_3\text{MnTiO}_7$.

DOI: [10.1103/PhysRevB.92.214416](https://doi.org/10.1103/PhysRevB.92.214416)

PACS number(s): 75.40.Cx, 75.47.Lx, 75.50.Lk, 75.50.Mm

I. INTRODUCTION

Materials exhibiting disordered/highly degenerate ground states, such as spin liquid, spin ice, or spin glass, are of paramount interest to the condensed matter physics community owing to their novel unconventional magnetic properties which sometimes demand a new physical model for understanding [1–5]. Geometric frustration and quenched disorder are the two major key elements which play important roles in driving such behavior by suppressing long-range magnetic order. While in the limit of strong frustration and low disorder, spin liquid excitation is expected to occur, disorder coupled frustration often leads to a spin glass state. Interestingly, there are few magnetic systems with geometric frustration, such as $\text{Tb}_2\text{Mo}_2\text{O}_7$ [6], $\text{Y}_2\text{Mo}_2\text{O}_7$ [7], $\text{Mn}_2\text{Sb}_2\text{O}_7$ [8], and $\text{Sr}_2\text{CaReO}_6$ [9], which exhibit extremely low disorder but show spin glass transition, although the origin of such an unconventional spin glass phase is unclear. A recent neutron scattering study of the single crystalline $\text{Y}_2\text{Mo}_2\text{O}_7$ has shown liquidlike correlations in the frozen state [10]. Therefore, the conventional assumption, “the stabilization of spin liquid or spin glass state is based on the subtle balance between frustration and disorder,” is not adequate to understand the unusual (observed) low temperature behavior. Moreover, recent theoretical calculations using density matrix renormalization group algorithms have shown that quantum spin liquids exhibit characteristic features of a particular class (\mathbb{Z}_2) of topological order such as fractional spinon ($s = \frac{1}{2}$, charge = 0) excitations [11]. In a striking similarity to the topological insulators whose properties, being topologically protected, are generally not affected by defects or disorder [12], it has been shown that the ground state properties of spin liquids are insensitive to disorder. For example, the substitution of up to 60% in the kagome compound $\text{SrCr}_{9p}\text{Ga}_{12-9p}\text{O}_{19}$ (SCGO) which is known to be a spin liquid, has no effect on the low temperature thermal and bulk magnetic properties [13]. Furthermore, the spin liquid state in SCGO has been reported to coexist with a spin glass state [14]. The presence of these

dual properties (spin glass and spin liquid state) has been explained on the basis of a simple model by describing the real material consisting of correlated spins with a fraction of uncorrelated spins called the orphan spins [15]. Therefore, the observed spin glass state in geometrically frustrated materials, such as SCGO [14], $\text{Tb}_2\text{Mo}_2\text{O}_7$ [16], and $\text{Y}_2\text{Mo}_2\text{O}_7$ [10], which coexists with liquidlike correlated spins, has been categorized as unconventional type spin glass state. On the other hand, chemical disorder when coupled with strong correlation gives rise to novel physical phenomena, such as non-Fermi liquid behavior [17]. One of the common aspects in the thermodynamic properties of these two kinds of systems is that the phase transition may be characterized by atypical critical exponents in the scaling behavior [18,19]. In pursuit of understanding the coexistence of disorder, frustration, and strong correlation, we have studied the low temperature magnetic and thermodynamic behavior of $\text{Sr}_3\text{MnTiO}_7$.

$\text{Sr}_3\text{MnTiO}_7$ (SMTO) belongs to the Ruddlesden-Popper (RP) phase ($A_{n+1}B_nO_{3n+1}$) with $n = 2$ in which disorder is inherently present in the material since the B site is occupied by two transition metals. The RP phases have drawn a lot of attention in the last decade owing to the colossal magnetoresistance effect in both $n = 1$ and $n = 2$ members [20,21]. However, the $n = 2$ members are particularly interesting as these exhibit two-dimensional transport and magnetic properties with high degrees of anisotropy [22]. The electronic band structure calculation of $\text{Sr}_3\text{Mn}_2\text{O}_7$ (SMO) has shown that Mn ions are antiferromagnetically coupled by interlayer and intralayer superexchange interactions [23]. Since SMTO also adopts the same crystal structure as SMO, antiferromagnetic interaction of Mn ions is expected in SMTO as well. In this paper, we have shown the absence of magnetic order in SMTO and the unusual low temperature magnetic properties, which correspond to the coexistence of both unconventional types, spin glass, and spin liquid states below 3.5 K.

II. EXPERIMENTAL DETAILS

A polycrystalline sample of SMTO was prepared by following the solid state reaction method as described in Ref. [24]. A stoichiometric mixture of high-purity (>99.95%)

*niharika@iitbbs.ac.in

precursors, SrCO_3 , Mn_2O_3 , and TiO_2 was pressed into pellets after homogenization by grinding. The heat treatment was carried out at 1273 K for 24 h followed by annealing at 1583 K for 50 h. To obtain the single phase sample, final sintering at 1633 K was repeated several times. The phase purity of the sample was examined by x-ray powder diffraction technique using PANalytical diffractometer with $\text{Cu-K}\alpha$ radiation. Magnetic and heat-capacity measurements were performed employing commercial Physical Property Measurement Systems (PPMS, Quantum Design). Neutron diffraction (ND) experiments were carried out at wavelength of 1.48 Å on the multi-position sensitive detector (PSD) based focusing crystal diffractometer (FCD) set up by UGC-DAE Consortium for Scientific Research, Mumbai Centre at the National Facility for Neutron Beam Research (NFNBR), Dhruva reactor (India). Several chunks of STMO pellet of about 5 mm were tightly packed in a vanadium can for measuring ND patterns [25]. Low temperature ND patterns were recorded by putting the sample inside a closed cyler refrigerator (AS Scientific Products, UK). All the ND patterns were analyzed using the FullProf Suite program for crystal and magnetic structures [26].

III. RESULTS AND DISCUSSIONS

The analysis of room-temperature powder x-ray diffraction (XRD) and ND data establishes the single phase nature of the specimen which crystallizes in a tetragonal structure with space group $I4/mmm$. The lattice parameters obtained from the refinement of ND and XRD data (shown in Fig. 1) are in good agreement with the reported results [24]. All the

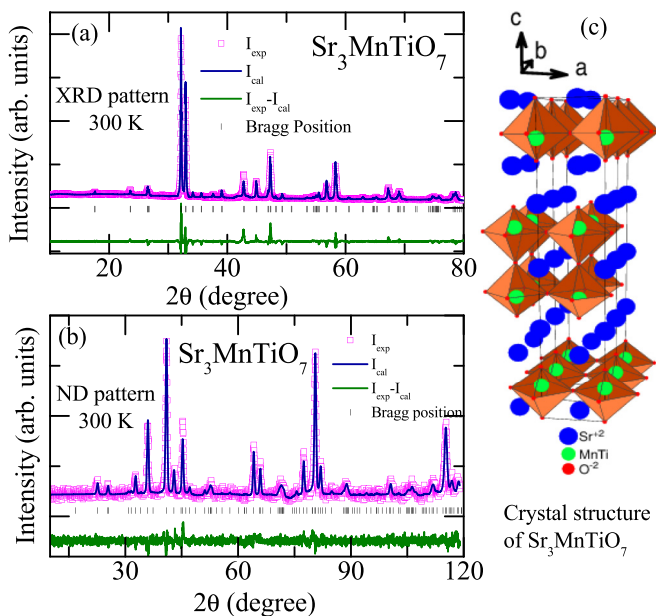


FIG. 1. (Color online) The room temperature (a) XRD pattern and (b) ND pattern of $\text{Sr}_3\text{MnTiO}_7$. Circles represent the experimental data, while the solid curve is the best fit from the Rietveld refinement using FULLPROF. The positions of Bragg reflections are marked by vertical lines. (c) Schematic presentation of the crystal structure of $\text{Sr}_3\text{MnTiO}_7$ showing the perovskite double layers in the ab plane which are separated by SrO layers along the c axis.

structural parameters obtained from the Rietveld refinement of ND data are available in the Supplemental Material [27]. The previous report has shown a possibility of mixed valence state of Mn (Mn^{3+} and Mn^{4+}) may be due to oxygen vacancies. As shown in Fig. 1, the crucial feature in the crystal structure of $\text{Sr}_3\text{MnTiO}_7$ is that there is stacking of sheets of bilayers of MO_6 ($M = \text{Mn}, \text{Ti}$) separated by a nonmagnetic SrO layer. Therefore, both $2b$ and $4e$ positions were occupied by Sr, while another $4e$ position was occupied by Mn and Ti. As described in the previous crystallographic studies on SMTO [24], the distortion of MO_6 octahedra may be attributed to the Jahn-Teller active ion Mn^{3+} .

We may recall that the mixed valence states of Mn in perovskite and bilayer manganites promote double exchange interaction resulting in colossal negative magnetoresistance, which has gained overwhelming attention in last decade [21,22]. However, the presence of mixed valence states of Mn in SMTO due to oxygen vacancies is quite different as it exhibits insulating behavior [24].

Figure 2(a) displays the temperature dependence of the magnetic susceptibility $\chi(T) (= M(T)/H)$ and its inverse measured in an applied field of 10 kOe. We note that $\chi(T)$ increases smoothly on cooling without any anomaly corresponding to magnetic phase transition at least down to 1.8 K. The inverse susceptibility is found to be linear in the high temperature range, i.e. above ~ 150 K. A Curie-Weiss fit to the data (> 150 K) yields an effective moment of $4.65 \mu_B/\text{Mn}$ and a Curie-Weiss temperature $\theta_{\text{CW}} = -427$ K. The value of the effective moment suggests a mixed-valence state for Mn with

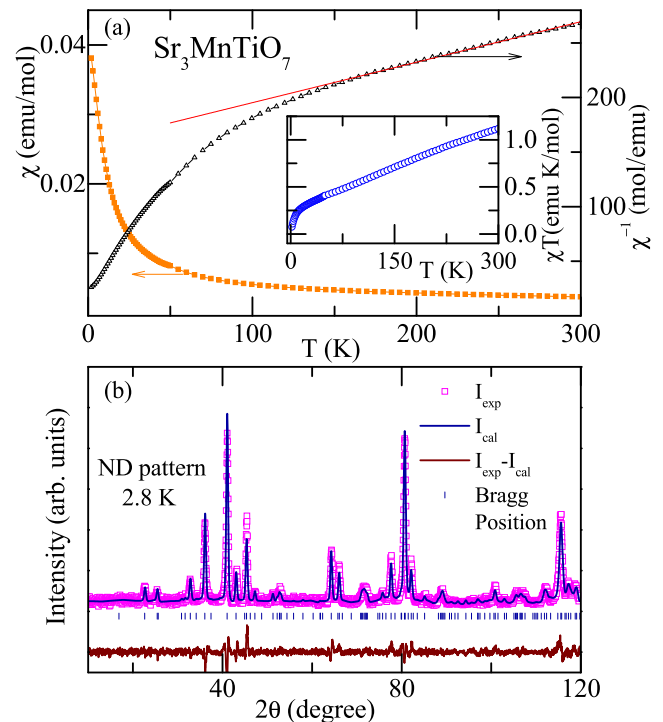


FIG. 2. (Color online) (a) Temperature dependence of magnetic susceptibility [$\chi(T)$] and inverse susceptibility of $\text{Sr}_3\text{MnTiO}_7$ in the presence of 10 kOe applied magnetic field. Inset shows the plot of $\chi(T)T$ as a function of temperature. (b) ND pattern of $\text{Sr}_3\text{MnTiO}_7$ measured at $T = 2.8$ K with a neutron wavelength of $\lambda = 1.48$ Å.

a major fraction ($\sim 75\%$) of Mn in Mn^{3+} state presumably due to oxygen deficiency and around 25% of Mn in Mn^{4+} state. From the calculated Curie-Weiss constant ($\theta_{\text{CW}} = -427$ K) and a decrease in χT vs T curve [shown in the inset of Fig. 2(a)] it may be inferred that the exchange coupling is large and predominantly antiferromagnetic. However, the absence of any magnetic ordering above 1.8 K indicates the presence of spin fluctuations may be due to geometrical frustration and/or Mn/Ti occupational disorder. As reported previously by theoretical calculation and analysis of the exchange interaction path in $\text{Sr}_3\text{Mn}_2\text{O}_7$, antiferromagnetic interaction within bilayer, intrabilayer and interbilayer may result in magnetic frustration in the system [23]. In SMTO, since Mn is the only magnetic ion which is placed at the 4e sites in the bilayers as shown in Fig. 1(c), magnetic frustration is likely to be present in the specimen. In spite of such a large θ_{CW} , absence of magnetic order may suggest a spin liquid behavior at the first instance. Therefore, we collected ND data at low temperature (2.8 K) to confirm the absence of long-range magnetic order. The low T data was successfully refined with the same tetragonal structure which is described at room temperature [see Fig. 2(b)]. There is no additional Bragg peak or discontinuity appearing at low temperature apart from the nuclear reflections, which rules out the occurrence of any structural or magnetic phase transition.

To further explore the magnetic properties, we have performed magnetization measurements after cooling the specimen in zero field (ZFC) as well as in field (FC) for various applied magnetic fields. For an applied field lower than 5 kOe, there is a difference between the ZFC and FC protocols below 5 K as shown in Fig. 3(a), which may indicate the presence of spin glass type state. For low fields (say 100 Oe or lower), the ZFC curve exhibits a well-defined peak around 3.5 K, while the FC curve continues to increase up to the lowest measured temperature instead of a smooth saturation (plateau) expected for a spin glass. This behavior suggests that there exists a fraction of spins which contribute to such a paramagnetic type rise in the FC behavior. Furthermore, we observe that the peak in the ZFC curve gradually smears out with increasing magnetic field strength, and the ZFC curve merges with the FC curve for fields of 5 kOe or higher. In order to shed light on the freezing behavior, we have plotted the temperature derivative of ZFC curves measured at various applied fields in Figs. 3(b) and 3(c). We find a sharp minimum in the $d(\chi)/dT$ curve for the lower applied fields corresponding to the freezing temperature $T_g = 3.5$ K. With increasing the strength of external magnetic field, the dip is found to be broadened and shifted towards higher temperature. This behavior is quite similar to the $d\chi/dT$ vs T features observed in $\text{SrCr}_9\text{pGa}_{12-9\text{p}}\text{O}_{19}$, which is considered to exhibit a spin singlet liquid state [28]. Moreover, the χ vs T behavior at various applied magnetic fields is also found to be similar to that of low Ti-doped $\text{Na}_4\text{Ir}_3\text{O}_8$ [29]. Thus, the ZFC-FC irreversibility along with the observed features is indicative of partial spin freezing in a background of a spin liquid state.

To ascertain the spin freezing behavior, magnetic field dependence of magnetization recorded at a few selected temperature in the ZFC condition of the specimen is depicted in Fig. 4(a). At the lowest measured temperature (1.8 K), we observe the Sigmoidal-shaped $M(H)$ curve with a negligibly

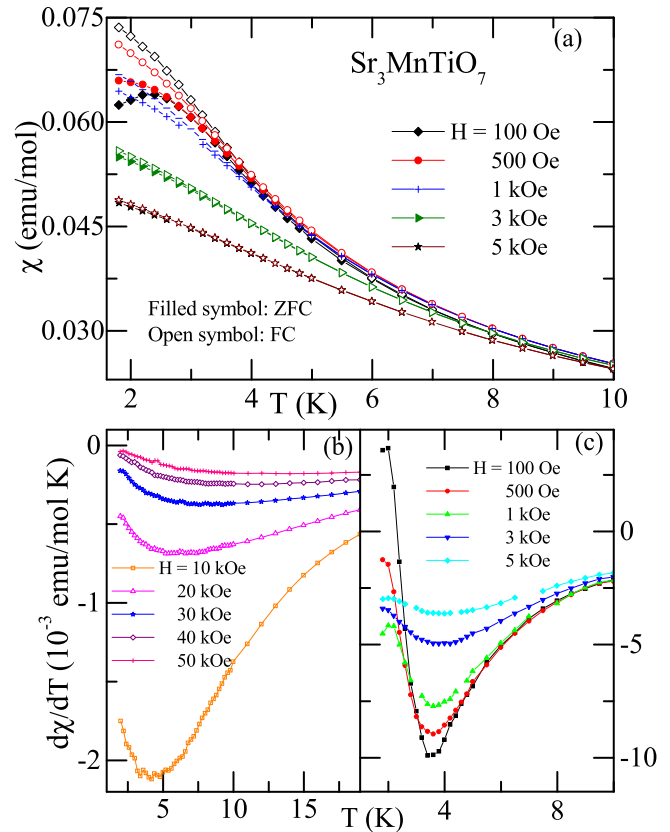


FIG. 3. (Color online) (a) The ZFC and FC magnetic susceptibility [$\chi(T)$] of $\text{Sr}_3\text{MnTiO}_7$ as a function of temperature measured in low applied magnetic fields. (b) and (c) The temperature derivation of $\chi(T)$ as a function of temperature at various applied fields.

small value of retentivity ($0.0001 \mu_B/\text{Mn}$) and coercive field (70 Oe), which indicates glassy magnetic behavior [30]. However, there is no trace of saturation in the $M(H)$ curve even for an applied field up to 90 kOe, and magnetization exhibits monotonic increase in H as though there is a paramagnetic component as well. This behavior also supports the inference drawn from susceptibility results that the low temperature spin glass type phase coexists with the paramagnetic phase. With increasing temperature, the low temperature S-shape curve gradually evolves into linear $M(H)$ behavior at 50 K, as expected in a paramagnetic state [see Fig. 4(b)]. The retentivity and coercivity also become negligibly small (comparable to the sensitivity of the magnetometer) at temperatures higher than 4 K. It is worth mentioning that the $M(H)$ value ($0.225 \mu_B/f.u.$) for an applied field of 90 kOe is much smaller than the theoretically calculated value using Brillouin function for paramagnetic spin ($3 \mu_B$ for $S = 3/2$ and $4 \mu_B$ for $S = 2$), suggesting the presence of correlated spins.

Since the spin glass system is generally characterized by a slow relaxation of magnetization in the frozen state, we have also performed thermoremanent magnetization (M_{TRM}) measurements at 1.8 K. To carry out TRM measurements, we first field cooled the specimen (in 500 Oe) from 100 to 1.8 K and recorded the time decay of magnetization after switching off the field. As illustrated in Fig. 4(c), M_{TRM} exhibits typical logarithmic relaxation behavior following the equation given

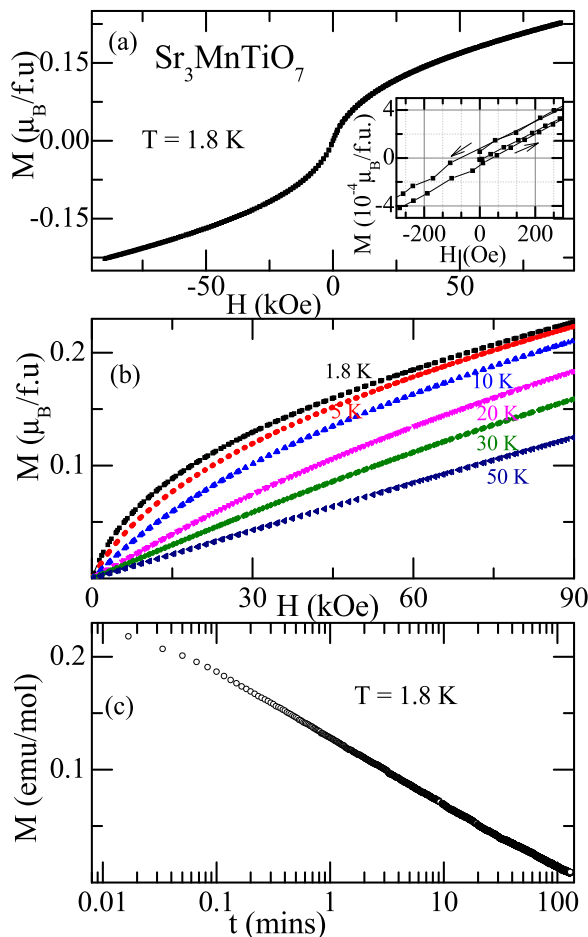


FIG. 4. (Color online) (a) and (b) Magnetic field dependence of magnetization measured at selected temperatures. Inset shows the expanded view of the M - H loop near the origin. (c) Time decay of thermoremanent magnetization (M_{TRM}) at $T = 1.8$ K.

below

$$M_{\text{TRM}} = M_0 - S \ln(t),$$

where M_0 is constant at given measuring field and S is called the magnetic viscosity which is related to the relaxation time. Such a logarithmic behavior has been observed in several spin glass systems [30] in which a large distribution of barrier energy exists.

In order to get further insight into the low T magnetic behavior, the heat capacity [$C(T)$] measurements were performed as a function of temperature in zero and applied magnetic fields, which is shown in Fig. 5(a). Here, $C(T)$ is found to decrease monotonically with decreasing temperature without exhibiting either a λ -type anomaly or any broad feature supporting magnetic phase transition or spin glasslike transition, respectively. Moreover, the $C(T)$ curves measured in the presence of magnetic field also overlap with the zero field data. However, an enlarged view of the low temperature part (see inset I) shows a pronounced field dependent feature which may provide evidence for the presence of magnetic entropy at low temperature. In the C/T vs T plot, shown in Fig. 5(b), we observe an upturn in the zero field data below 5 K with a small peak at ~ 2.5 K. By increasing the strength of the magnetic

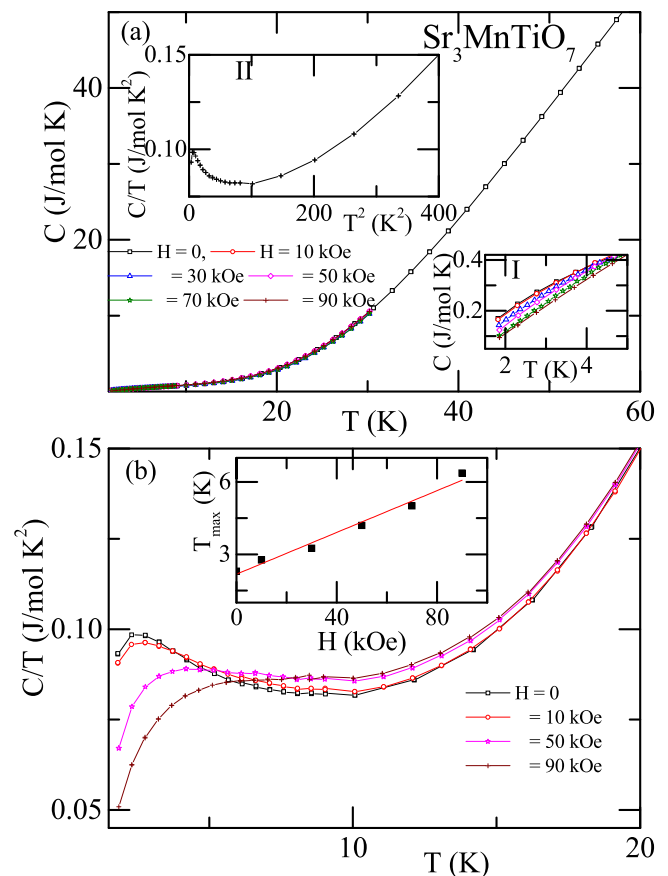


FIG. 5. (Color online) (a) Heat capacity (C) of $\text{Sr}_3\text{MnTiO}_7$ as a function of temperature in the presence of various external magnetic fields. Inset I shows the variation of C/T as a function of T^2 . Inset II shows an expanded view of $C(T)$ at low temperature region. (b) Temperature variation of C/T around the transition region. Inset shows the dependence of T_{max} (as described in the text) on the magnetic field.

field, this upturn gets suppressed, while the peak broadens and shifts towards higher temperature. We have plotted T_{max} as a function of magnetic field H in the inset of Fig. 5(b), which shows essentially a linear behavior. This linear dependence of T_{max} is a characteristic feature seen in the quantum spin liquid candidate $\text{ZnCu}_3(\text{OH})_6\text{Cl}_2$ [30]. Furthermore, the field dependent behavior resembles that of a lightly doped spin liquid phase $\text{Na}_4(\text{Ir}_{0.9}\text{Ti}_{0.1})_3\text{O}_8$ [29]. The partial substitution of nonmagnetic Ti in the spin liquid phase $\text{Na}_4\text{Ir}_3\text{O}_8$ is believed to generate orphan spins which prompt such a glassy feature.

Since the striking features seen in the above results, such as (i) the absence of long-range magnetic order as confirmed from low T neutron diffraction, magnetic susceptibility, and heat capacity data; (ii) irreversibility in ZFC-FC profile below $T_g \sim 3.5$ K only at low fields; (iii) negligibly small hysteresis; and (iv) slow relaxation of magnetization below T_g suggests a spin glass transition, although specific contradiction to the conventional spin glass behavior, e.g., absence of a broad peak in $C(T)$ just above T_g and plateau in FC susceptibility exist; we consider it essential to examine the critical exponents corresponding to this thermodynamic transition. Moreover, the frustration parameter (θ_{CW}/T_g) turned out to be 122, which is

much larger than the conventional spin glasses (typically <5). Therefore, we discuss below the scaling behavior of magnetization to understand and explore the freezing mechanism since the static susceptibility in particular nonlinear susceptibility is sensitive to the freezing order parameter.

The contribution of nonlinear susceptibility to χ_{dc} can be extracted from the temperature and field dependence of magnetization above T_g , which is generally expressed in terms of the odd powers of the magnetizing field [7,18,19,30]

$$\begin{aligned} M(T, H) &= \chi_0(T)H - a_3(T)(\chi_0 H)^3 + a_5(T)(\chi_0 H)^5 - O(H^7) \\ &= \chi_0(T)H - \chi_3(T)(H)^3 + \chi_5(T)(H)^5 - O(H^7), \end{aligned} \quad (1)$$

where the coefficient χ_0 represents the linear susceptibility and all other coefficients of higher-order terms correspond to the nonlinear contribution. Therefore, the total nonlinear part of the magnetic susceptibility can be defined as

$$\chi_{nl}(T, H) = 1 - \frac{M(T, H)}{\chi_0(T)H}. \quad (2)$$

Since the linear susceptibility term is nondivergent at the thermodynamic (spin glass) transition temperature, the behavior of χ_{nl} has important implications in determining the critical exponents which diverge near the critical temperature following the power law

$$\chi_{nl} \propto \tau^{-\gamma}, \quad (3)$$

where $\tau (= \frac{T}{T_g} - 1)$ is the reduced temperature, and $\gamma (>0)$ is the static critical exponent. Furthermore, the nonlinear susceptibility diverges at T_g with a power law dependence on H

$$\chi_{nl}(T = T_g) \propto H^{2/\delta}, \quad (4)$$

where δ is the second static critical exponent characterizing the spin glass transition.

Finally, the most relevant test describing the critical behavior of a spin glass transition may be obtained by the single parameter scaling relationship of χ_{nl}

$$\chi_{nl}(T, H) = H^{2/\delta} f(\tau^{(\gamma+\beta)/2}/H), \quad (5)$$

where β is the spin glass order parameter critical exponent. The scaling function $f(x)$ can be arbitrarily chosen, provided it must satisfy the following asymptotic boundary conditions: $f(x) = \text{constant}$ as $x \rightarrow 0$ and $f(x) = x^{-\frac{2\gamma}{\gamma+\beta}}$ as $x \rightarrow \infty$. These boundary conditions correlate Eq. (5) with Eqs. (3) and (4) by providing physical meaning to the mathematical relation. Moreover, the two independent exponents γ and δ can be related through the hyperscaling relation

$$\delta = 1 + \frac{\gamma}{\beta}. \quad (6)$$

To apply the above formalism, we extracted χ_{nl} from the magnetization data which were collected with much care under the field cooled condition as described in Ref. [7]. The specimen was first cooled from room temperature to 15 K in zero field, and then a magnetic field in the range of 30 – 10⁴ Oe was switched on. Keeping H constant, M_{FC} vs T was measured in the T range 2–15 K following a slow cooling at a rate of 5 mK/s. Before switching on the next field, the sample was again warmed up to 15 K without making the field

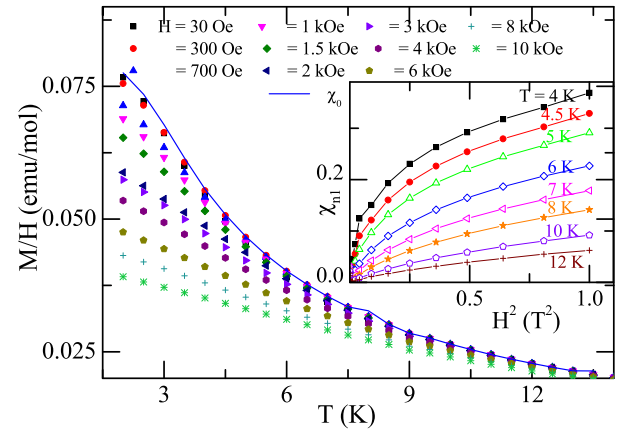


FIG. 6. (Color online) Field cooled magnetic susceptibility of $\text{Sr}_3\text{MnTiO}_7$ measured under slow cooling condition as described in the text. Solid line corresponds to the linear susceptibility χ_0 , obtained by fitting the experimental data to Eq. (1). Inset shows the net nonlinear susceptibility χ_{nl} as a function of H^2 for selected temperatures.

zero. As described earlier [7,18], this procedure minimizes the influence of magnetic hysteresis of the superconducting magnet (used in the magnetometer) on the measured data. For the same reason, the field was never decreased to zero during the entire measurement period. Figure 6 shows the temperature variation of FC magnetic susceptibility (M/H) for various applied magnetic fields. It is evident from the figure that the nonlinear contribution to M/H increases by decreasing the temperature towards T_g . In order to deduce χ_0 and χ_3 , the $M(H, T)$ data was plotted as a function of H^2 and fitted with the Eq. (1). Since, at lower fields, the first two terms in the right-hand side of Eq. (1) are dominant, we neglected the terms with H^5 and higher while performing the fitting, which was restricted to the low field range only. The value of χ_0 obtained from this fit at various temperatures is shown by the solid line in the main panel of Fig. 6. Again, by using Eq. (2), the net nonlinear part of M/H was evaluated at various temperatures close to T_g which is shown against H^2 in the inset of Fig. 6. This plot indicates the enhancement of the curvature as one approaches towards T_g .

Figure 7(a) shows the log-log plot of $a_3 (= \chi_3/\chi_0^3)$ vs τ for different choices of T_g in the range (2–6 K). The value of γ was estimated from the linear fit of $\log a_3$ vs $\log \tau$ which varies in the range (1.5–0.6) as shown in the left panel of the inset of Fig. 7(a). In the same inset (right panel), we have also shown the goodness of fitting for different choices of T_g . As can be seen in the figure, the best fit was obtained for $T_g = 3.5$ K, which is also consistent with the minimum in $d\chi/dT$ for low applied fields [see inset of Fig. 3(b)]. It is to be noted that the extracted value of $\gamma = 1.1$ corresponding to $T_g = 3.5$ K is comparatively smaller than that expected for a conventional (disordered) spin glass system [29,31].

Next, the second critical exponent δ was determined from the linear fitting of $\ln \chi_{nl}(T_g)$ vs $\ln H$ as depicted in the inset of Fig. 7(b), which was turned out to be 3.2. If we consider SMTO to undergo a true equilibrium phase transition at $T_g \sim 3.5$ K, the spin glass order parameter β should take

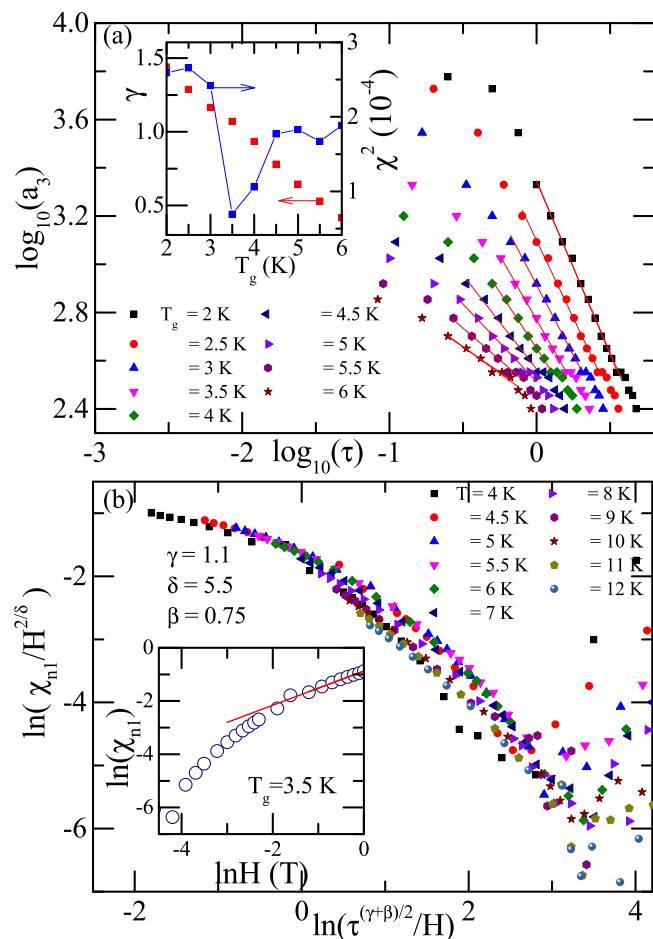


FIG. 7. (Color online) (a) Plot of the logarithm of $a_3 (= \chi_3/\chi_0^3)$ as a function of logarithm of $\tau (= \frac{T}{T_g} - 1)$ for different choices of T_g . The inset shows the goodness of fitting parameter χ^2 (right panel) and the critical exponent γ (left panel) for the chosen values of T_g . (b) Scaling behavior of the net nonlinear susceptibility χ_{nl} for $\text{Sr}_3\text{MnTiO}_7$ according to Eq. (5) for the T range (4–12) K. The inset shows the log-log plot of χ_{nl} vs H corresponding to $T_g = 3.5$ K.

the value $[\gamma/(\delta - 1)] = 0.5$. However, with these exponent values, the scaling behavior of χ_{nl} as described in Eq. (5) could not be achieved. Therefore, in an attempt to make the χ_{nl} data collapsing into a single curve, we varied the critical exponents δ and β while keeping γ and T_g fixed at 1.1 and 3.5 K. It is apparent from Fig. 7(b) that the scaling behavior can be well described by a single curve with exponents $\delta = 5.5$, $\gamma = 1.1$, $\beta = 0.75$, and $T_g = 3.5$ K, although the hyperscaling relation between the exponents as given in Eq. (6) is not fulfilled. Since the above analysis resulted in different values of the exponents from the asymptotic power law singularity of χ_{nl} and divergence of χ_{nl} near T_g , the transition observed at 3.5 K is not necessarily a true equilibrium spin glass transition. Moreover, the values of the exponents are found to be different than those reported for conventional spin glasses [30,32]. It is also to be noted that there is no shifting of the ac susceptibility peak towards high temperature by increasing the probing frequency (see Supplemental Material [27]). In view of this, we wonder whether the spin glass transition observed in SMTO may be considered as an unconventional type as seen in the spin liquid

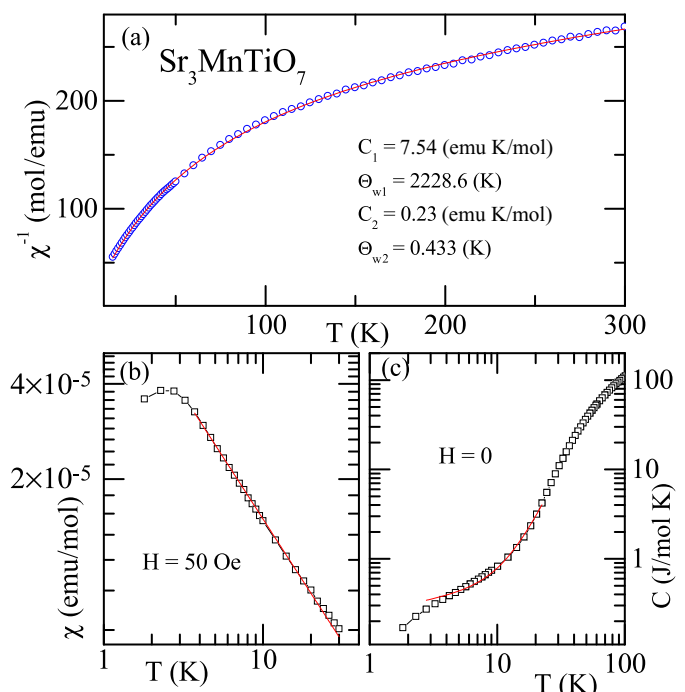


FIG. 8. (Color online) (a) The inverse susceptibility of $\text{Sr}_3\text{MnTiO}_7$ and a fit (solid line) to the expression predicted for the two-population model (as described in the text). Power law dependence of (b) low field magnetic susceptibility (χ_{dc}) and (c) zero field heat capacity (C) on temperature as described in the text.

candidate SCGO [19] and the compound exhibiting liquidlike spin correlation $\text{Tb}_2\text{Mo}_2\text{O}_7$ [18].

At this juncture, it is worth recalling the two-population model proposed by Schiffer and Daruka [15] to explain the magnetic susceptibility behavior of SCGO and other frustrated spin systems. By considering the existence of two separate spin states corresponding to the correlated spins and orphan spins, they could successfully describe the anomalous experimental data. This concept was further supported by Sen *et al.* [5] by developing an analytical theory which accounts for both entropic and energetic effects. One of the important conclusions drawn from this theory is that a spin defect gets screened in a background of frustrated magnets (spin liquid).

As many of the experimental features in $\chi(T)$ and $C(T)$ of SMTO are reminiscent to the behavior of $\text{Na}_4(\text{Ir}_{0.9}\text{Ti}_{0.1})_3\text{O}_8$ and SCGO, we propose the coexistence of two different spin states in SMTO corresponding to the correlated spins and uncorrelated spins in an analogy to the above mechanism.

To support this claim, we have analyzed the susceptibility data in light of the two-population model taking into account the contributions from correlated and uncorrelated spins. Under these circumstances, the inverse susceptibility is expected to follow; $\chi^{-1}(T) = [\frac{C_1}{T - \Theta_{w1}} + \frac{C_2}{T - \Theta_{w2}}]$, where C_1 , Θ_{w1} , and C_2 , Θ_{w2} correspond to the Curie constant and Weiss temperature of correlated spins and orphan spins, respectively [15]. As shown in the Fig. 8(a), the agreement of the $\chi^{-1}(T)$ data of SMTO with the two-population model is found to be excellent. The parameters C_1 , Θ_{w1} , and C_2 , Θ_{w2} obtained from the fit are also shown in the same figure. It may be noted that $C_1 \gg C_2$, as expected and also observed in most of the

frustrated magnetic systems [15], which basically implies the fraction of correlated spins is much higher than that of orphan spins. In the same line, we also obtain Θ_{w2} as extremely low (~ 0.433 , equally good fit was obtained by setting Θ_{w2} as zero) in comparison to Θ_{w1} , which indicates effective exchange field of the correlated spins.

In order to get further evidence of correlated spins, we examined the power law dependence of magnetic susceptibility and heat capacity. The $\chi_{dc}(T)$ measured at extremely low applied field (40 Oe) was used for this analysis as it may be a crude approximation to the ac susceptibility behavior. In the T range immediately above T_g , $\chi(T)$ follows a power law scaling behavior, $\chi(T) \propto T^{-\beta}$, with $\beta = 0.76$ as shown in Fig. 8(b). With increasing the applied magnetic field, both the T range of this fitting and the exponent β are found to decrease. In Fig. 8(c), we have shown the apparent power law scaling of $C(T)$ in the region $20\text{ K} > T > T_g$ by fitting with the equation $C = AT^3 + BT^{1-\alpha}$, where the first term is due to the lattice contribution and second due to power law scaling. The best fit is obtained for $\alpha = 0.72$. While describing the scaling properties of Herbertsmithite which is considered as the best example of quantum spin liquid, Shaginyan *et al.* [31] have shown non-Fermi liquid behavior in magnetic susceptibility and heat capacity similar to that of through heavy Fermion system for which $\alpha = \beta = 0.67$. The small deviation of exponent values observed for SMTO may be attributed to the additional contribution arising from the uncorrelated spin phase.

IV. CONCLUSIONS

To conclude, we present a comprehensive study of the low temperature magnetic and thermodynamic properties of the RP phase $\text{Sr}_3\text{MnTiO}_7$. Although, the occurrence of a spin glass

type transition at ~ 3.5 K was anticipated by an irreversibility of low field ZFC-FC curves, low magnetic hysteresis, and slow relaxation of thermoremanent magnetization, the critical exponents derived from the T and H dependence of nonlinear susceptibility do not comply with the hyperscaling relation. Therefore, the deduced scaling behavior indicates a mere mathematical fitting which lacks physical meaning. Moreover, we find many experimental features in $\chi(T)$ and $C(T)/T$ resembling the behavior of spin liquids or lightly doped spin liquids. In addition, the absence of a magnetic Bragg peak in the low temperature ND profile of $\text{Sr}_3\text{MnTiO}_7$ supports the existence of a spin glass/spin liquid state. In light of the key findings of our results and analysis, such as absence of magnetic order and unconventional scaling behavior, we suggest the presence of both spin glass (uncorrelated spins which freeze) and spin liquid (correlated spins) states similar to the two-population model suggested by Schiffer and Daruka [15]. We emphasize that the structural distortion of MO_6 octahedra and random distribution of $\text{Mn}^{3+}/\text{Mn}^{4+}$ might be responsible for the observed spin glass behavior. However, direct probe methods, such as μSR and inelastic neutron scattering studies, may be more useful in order to establish the origin of such behavior. Additionally, the study of SMTO may provide an important insight into the spin liquid physics arising out of disorder and frustration.

ACKNOWLEDGMENTS

The neutron diffraction work was carried out under the Collaborative research scheme project (No. CRS-M-167) of the UGC-DAE CSR, Mumbai Centre. N.M. acknowledges financial support from Department of Science and Technology, India, under the Fast Track scheme (Ref. No. SR/FTP/PS-164/2011).

-
- [1] L. Balents, *Nature* **464**, 199 (2010).
- [2] G. Jackeli and G. Khaliullin, *Phys. Rev. Lett.* **102**, 017205 (2009).
- [3] J. T. Chalker, P. C. W. Holdsworth, and E. F. Shender, *Phys. Rev. Lett.* **68**, 855 (1992).
- [4] M. Nifle and H. J. Hilhorst, *Phys. Rev. Lett.* **68**, 2992 (1992).
- [5] A. Sen, K. Damle, and R. Moessner, *Phys. Rev. Lett.* **106**, 127203 (2011).
- [6] B. D. Gaulin, J. N. Reimers, T. E. Mason, J. E. Greedan, and Z. Tun, *Phys. Rev. Lett.* **69**, 3244 (1992).
- [7] M. J. P. Gingras, C. V. Stager, N. P. Raju, B. D. Gaulin, and J. E. Greedan, *Phys. Rev. Lett.* **78**, 947 (1997).
- [8] H. D. Zhou, C. R. Wiebe, A. Harter, N. S. Dalal, and J. S. Gardner, *J. Phys: Condens. Matter* **20**, 325201 (2008).
- [9] J. E. Greedan, S. Derakhshan, F. Ramezanipour, J. Siewenie, and Th. Proffen, *J. Phys: Condens. Matter* **23**, 164213 (2011).
- [10] H. J. Silverstein, K. Fritsch, F. Flicker, A. M. Hallas, J. S. Gardner, Y. Qiu, G. Ehlers, A. T. Savici, Z. Yamani, K. A. Ross, B. D. Gaulin, M. J. P. Gingras, J. A. M. Paddison, K. Foyevtsova, R. Valenti, F. Hawthorne, C. R. Wiebe, and H. D. Zhou, *Phys. Rev. B* **89**, 054433 (2014).
- [11] S. Yan, D. A. Huse, and S. R. White, *Science* **332**, 1173 (2011).
- [12] B. A. Bernevig, L. H. Taylor, and S.-C. Zhang, *Science* **314**, 1757 (2007).
- [13] A. P. Ramirez, G. P. Espinosa, and A. S. Cooper, *Phys. Rev. Lett.* **64**, 2070 (1990).
- [14] C. Broholm, G. Aeppli, G. P. Espinosa, and A. S. Cooper, *Phys. Rev. Lett.* **65**, 3173 (1990); S.-H. Lee, C. Broholm, G. Aeppli, T. G. Perring, B. Hessen, and A. Taylor, *ibid.* **76**, 4424 (1996); Y. J. Uemura, A. Keren, K. Kojima, L. P. Le, G. M. Luke, W. D. Wu, Y. Ajiro, T. Asano, Y. Kuriyama, M. Mekata, H. Kikuchi, and K. Kakurai, *ibid.* **73**, 3306 (1994).
- [15] P. Schiffer and I. Daruka, *Phys. Rev. B* **56**, 13712 (1997).
- [16] M. J. Harris, M. P. Zinkin, Z. Tun, B. M. Wanklyn, and I. P. Swainson, *Phys. Rev. Lett.* **73**, 189 (1994).
- [17] E. Miranda and V. Dobrosavljevic, *Rep. Prog. Phys.* **68**, 2337 (2005).
- [18] D. K. Singh and Y. S. Lee, *Phys. Rev. Lett.* **109**, 247201 (2012).
- [19] B. Martínez, A. Labarta, R. Rodríguez-Solá, and X. Obradors, *Phys. Rev. B* **50**, 15779 (1994).
- [20] Y. Moritomo, A. Asamitsu, H. Kuwahara, and Y. Tokura, *Nature* **380**, 141 (1996).

- [21] T. Kimura, Y. Tomioka, H. Kuwahara, A. Asamitsu, M. Tamura, and Y. Tokura, *Science* **274**, 1698 (1996).
- [22] R. Osborn, S. Rosenkranz, D. N. Argyriou, L. Vasiliu-Doloc, J. W. Lynn, S. K. Sinha, J. F. Mitchell, K. E. Gray, and S. D. Bader, *Phys. Rev. Lett.* **81**, 3964 (1998).
- [23] H. Meskine, Z. S. Popovic, and S. Satpathy, *Phys. Rev. B* **65**, 094402 (2002).
- [24] I. B. Sharma, C. Singh, and D. Singh, *J. Alloys and Compounds* **375**, 11 (2004).
- [25] V. Siruguri, P. D. Babu, M Gupta, A. V. Pimpale, and P. S. Goyal, *Pramana* **71**, 1197 (2008).
- [26] T. Roisnel and J. Rodriguez-Carvajal WINPLOTR, Laboratoire Léon Brillouin (Centre d'études atomiques-Centre national de la recherche scientifique), Centre d'études de Saclay, 91191 Gif-sur-Yvette Cedex (France) and Laboratoire de Chimie du Solide et Inorganique Moléculaire (UMR 6511), Université de Rennes 1, 35042 Rennes Cedex (France). <http://www-llb.cea.fr/fullweb/winplotr/winplotr.htm>; H. M. Rietveld, *J. Appl. Cryst.* **2**, 65 (1969).
- [27] See Supplemental Material at <http://link.aps.org/supplemental/10.1103/PhysRevB.92.214416> for crystallographic parameters obtained from the Rietveld refinement of the neutron diffraction data and the results of ac-susceptibility measurements.
- [28] A. P. Ramirez, B. Hessen, and M. Winklemann, *Phys. Rev. Lett.* **84**, 2957 (2000).
- [29] Y. Okamoto, M. Nohara, H. Aruga-Katori, and H. Takagi, *Phys. Rev. Lett.* **99**, 137207 (2007).
- [30] J. A. Mydosh, *Spin Glasses: An experimental Introduction* (Taylor and Frances, London) (1993). K. Binder and A. P. Young, *Rev. Mod. Phys.* **58**, 801 (1986).
- [31] V. R. Shaginyan, A. Z. Msezane, and K. G. Popov, *Phys. Rev. B* **84**, 060401 (2011).
- [32] H. Bouchiat, *J. Phys. (Paris), Lett.* **47**, 71 (1987).